PAPER

Check for updates

A metal–organic framework and conducting polymer based electrochemical sensor for high performance cadmium ion detection†

Yang Wang,*[ab] Lu Wang,[a] Wei Huang,[a] Ting Zhang,[a] Xiaoya Hu,[a] Jason A. Perman[b] and Shengqian Ma [ID] *[b]

In this work, a conductive electrochemical sensor, UiO-66-NH$_2$@PANI, was successfully prepared by polymerizing the conductive polyaniline (PANI) polymer around the metal–organic framework UiO-66-NH$_2$. Fourier transform infrared spectra, X-ray diffraction patterns, and X-ray photoelectron spectral data support the formation of UiO-66-NH$_2$@PANI. Additionally, scanning and transmission electron microscopy investigations confirm that PANI uniformly coated the surface of UiO-66-NH$_2$. The resultant material was applied to construct a novel electrochemical sensor for the reliable detection of cadmium ions due to the chelation mechanism between metal cations and amine groups. Under optimized conditions, a linear detection of Cd^{2+} concentration range of 0.5–600 µg L^{-1} was repeatable with a 0.3 µg L^{-1} lowest level detection limit. Little to no interference effects from other co-existing ions allow the sensor to work in varying environments for practical application. This method of coating metal–organic frameworks may show utility for constructing highly sensitive electrochemical sensors for the detection of heavy metal ions and more.

1. Introduction

In recent years, the release of harmful heavy metal ions into the environment has attracted great attention worldwide because of their toxicity and widespread use. Cadmium is among the most toxic heavy metals, even at very low concentrations causing a large number of health issues, including heart disease, cancer, and diabetes.[1–3] The limits established by the World Health Organization (WHO) and United States (US) Environmental Protection Agency (EPA) are 3 and 5 ppb.[4] Due to its high toxicity and very high bioaccumulation factor in the food chain, the development of reliable and sensitive methods for the determination of cadmium ions at trace concentrations is of particular importance to public health and environmental pollution control.

Several analytical techniques based on mesoporous materials including atomic absorption spectrometry, atomic emission spectrometry, inductively coupled plasma mass spectrometry, and anodic stripping voltammetry have been used for metal ion analysis.[5–8] Electrochemical stripping voltammetry has been recognized as a selective and sensitive technique for the detection of trace heavy metals because it involves an effective preconcentration step with advanced electrochemical measurement of the accumulated analytes.[9–11] However, being the heart of electrochemical sensors, most electrode materials have a number of limitations, such as low surface areas, lack of structural design, and the limited possibility for surface modification at which the electron transfer process occurs. Hence, recent efforts on electrode materials have been devoted to designing advanced materials with well-defined chemical and physical properties to improve electrochemical performances.

Over the past decades, the development in the design of metal–organic frameworks (MOFs) with high surface areas, uniform pores and chemical tunability has made possible important advances in materials science.[12,13] These characteristics make MOFs unique materials with the potential for diverse applications.[14–17] However, the use of MOFs as novel electrode materials has been underexplored due to multiple issues of poor conductivity and instability in aqueous solution for the majority of MOFs. In this regard, coupling MOFs with carbon materials, such as carbon spheres,[18] macroporous carbon,[19] and metal nanoparticles (Au,[20] and Pt[21]), has been demonstrated as an effective approach to improve the mechanical strength and conductive performance of MOFs, and they have shown some promise as electrochemical biosensors. Nevertheless, because these materials always suffer from a complicated synthesis process, their wider practical applications are greatly inhibited in the electrochemical field.

[a] School of Chemistry and Chemical Engineering, Yangzhou University, Yangzhou 225002, China. E-mail: wangyzu@126.com

[b] Department of Chemistry, University of South Florida, 4202 East Fowler Avenue, Tampa, Florida 33620, USA. E-mail: sqma@usf.edu

† Electronic supplementary information (ESI) available: Experiment parameters and interference experiment. See DOI: 10.1039/c7ta01066d

Several conducting polymers find a variety of applications in sensing technology, which exhibit interesting electrical properties such as their ability to oxidize and reduce at a specific electrochemical potential.[22,23] Polyaniline (PANI) is known as one of the most promising conducting polymers due to its ease of preparation, relatively high conductivity, and good stability in the presence of water. The preparation of PANI with other materials to form solid composites has been the subject of considerable research interest, as they are expected to have combined properties of both solid composites and organic molecules.[24–26] In this work, we present a MOFs@PANI composite material prepared by loading PANI onto the surface of a MOF. UiO-66-NH$_2$ is constituted by hexameric Zr$_6$O$_{32}$ units and 2-amino-terephthalate linkers and characterized by alternating octahedral and tetrahedral cages sharing triangular windows.[27] Its potential applications were demonstrated on a photocatalyst,[28] adsorbent,[29] and acid-base catalyst.[30] Due to good water and chemical stability, and the abundance of amine groups, UiO-66-NH$_2$ was selected as a representative MOF support. PANI can effectively enhance the conductivity of composite materials by speeding up the electron/ion diffusion in the matrix. UiO-66-NH$_2$ not only serves as the backbone for PANI, but also provides a high surface area and more adsorption sites. The electrochemical performances of the UiO-66-NH$_2$@PANI composite material were evaluated in the context of detecting cadmium ions in aqueous solution. Various experimental parameters that affect the sensitivity of the UiO-66-NH$_2$@PANI modified electrode were optimized. Analytical applications of the sensor were demonstrated by environmental monitoring and biological testing.

2. Experimental section

2.1. Apparatus

A CHI660A electrochemical workstation (Chenhua Instrument, Shanghai, China) was used for voltammetric measurements with a three-electrode system. The working electrode was the UiO-66-NH$_2$@PANI modified glassy carbon electrode (GCE). The counter electrode was a platinum wire and the reference was an Ag/AgCl electrode. The powder X-ray diffraction (XRD) patterns were collected with a D8 Advance X-ray diffractometer (Bruker Co., Germany) from 5° to 80°. The scanning electron micrograph (SEM) images were obtained with a S-4800 microscope (Hitachi, Japan) at 15 KV. The transmission electron microscopy (TEM) images were obtained with a Tecnai 12 (Holland Philips) at 120 KV. The FTIR spectra were obtained with a Cary 610/670 infrared microspectrometer (Varian, America). The X-ray photoelectron spectroscopy data were collected using an ESCALAB 250Xi X-ray photoelectron spectroscope (Thermo Scientific, America) and calculated using linear fitting by Avantage of Thermo Scientific software. Specific surface area (BET) was measured on an automated NOVA/4000 E physical adsorption instrument by N$_2$ sorption at 77 K (Quantachrome). Thermogravimetric analysis was carried out in the temperature range of 50–800 °C at a heating rate of 10 °C min^{-1} in an air atmosphere with a flow rate of 30 mL min^{-1} using a Q500 (TA Instruments). High-resolution transmission electron micrographs (HRTEMs) were obtained with a FEI Tecnai G2 F30 S-TWIN field-emission transmission electron microscope (USA) at an acceleration voltage of 300 kV. Raman spectra were recorded using a Renishaw InVia microRaman system. The differential pulse voltammetry (DPV) measurements were recorded from −1.0 to −0.3 V with a pulse amplitude of 50 mV and a width of 50 ms. The electrochemical impedance spectroscopy (EIS) analysis was performed by using an Autolab PGSTAT30 (The Netherlands) using a solution of 0.1 M KCl containing 1.0 mM K$_3$[Fe(CN)$_6$]/K$_4$[Fe(CN)$_6$]. The amplitude of the applied sine wave potential was 5 mV and the frequency range was from 0.1 to 10 kHz at a bias potential of 190 mV.

2.2. Reagents and materials

A 0.02 mg L^{-1} cadmium stock solution was prepared by dissolving 0.6624 g CdCl$_2$ (Jinshan Chemicals, Shanghai, China) in 100.0 mL 1% (v/v) nitric acid. Working standard solutions were obtained by step-wise dilution. Hydrochloric acid, N,N-dimethylformamide (DMF), anhydrous ethanol, aniline (99%), ammonium peroxydisulfate (APS), zirconium tetrachloride (ZrCl$_4$), and 2-aminoterephthalic acid (H$_2$ATA) were purchased from Sinopharm Chemical Reagent Co., Ltd. (Shanghai, China). 0.1 mol L^{-1} acetate buffer solution (ABS, pH = 5.0) was prepared by mixing the appropriate amounts of sodium acetate and acetic acid. Double deionized water (18 MΩ cm^{-1}) was prepared by using a Milli-Q water purification system (Millipore, Bdfedford, MA, USA). Nitrogen gas (99.999%) was used for purging oxygen in a solution to provide an inert atmosphere.

2.3. Synthesis of UiO-66-NH$_2$

The UiO-66-NH$_2$ was prepared from a hydrothermal synthesis procedure after a minor modification.[28] ZrCl$_4$ (0.2332 g, 1 mmol) and 2-NH$_2$-benzenedicarboxylate (0.1812 g, 1 mmol) were dissolved into 50 mL DMF with ultrasonic vibration for 30 min. The mixed solution was transferred to a 100 mL Teflon-lined stainless steel autoclave and then maintained at 120 °C for 48 h in an oven. After the reaction, the autoclave was cooled to room temperature and the resulting solids were centrifuged and washed with anhydrous alcohol 5 times to remove any residual solvent. Subsequently the sample was vacuum dried at 100 °C for 12 h.

2.4. Synthesis of UiO-66-NH$_2$@PANI

UiO-66-NH$_2$ (0.3 g) was well-dispersed in 15 mL of 1 mol L^{-1} hydrochloric acid. Aniline (30 µL) monomer was then added to the above mixture and then ultrasonicated for 20 min. Afterwards, 0.114 g APS in 5 mL of 1 mol L^{-1} hydrochloric acid was added dropwise into the above solution at 0 °C, and then the mixture was stirred overnight to ensure complete polymerization. The resulting precipitates were centrifuged and rinsed three times with doubly distilled water and alcohol in turns. Finally, the obtained products were dried in a vacuum oven at 60 °C for 24 h. The pristine PANI was prepared in the same way but without the addition of UiO-66-NH$_2$ into the mixture of aniline and hydrochloric acid.

2.5. Preparation of modified electrode

The bare GCE was polished carefully with 0.5 and 0.03 μm alumina slurry and cleaned successively with ethanol and double distilled deionized water by sonication, and finally dried in a N_2 stream. After cleaning, 1.0 mg UiO-66-NH_2@PANI was ultrasonically dispersed into 1.0 mL DMF to form a homogeneous solution. 5.0 μL UiO-66-NH_2@PANI solution was placed onto the GCE surface, and dried under an infrared lamp. The obtained UiO-66-NH_2@PANI modified electrode was stored in air at room temperature.

3.   Results and discussion

3.1.   Characterization of materials

XRD patterns of PANI, UiO-66-NH_2, and UiO-66-NH_2@PANI are shown in Fig. 1. The two broad peaks of PANI at 20° and 25° 2θ represent the parallel (100) and perpendicular (110) periodicities of the PANI chain.[29] For the as-prepared UiO-66-NH_2, the experimental XRD pattern matches the calculated XRD pattern confirming its phase purity.[27] The final composite of UiO-66-NH_2@PANI displayed a similar XRD pattern as UiO-66-NH_2 with slight differences in peak intensities. Furthermore, the XRD pattern of UiO-66-NH_2@PANI did not exhibit the characteristic diffraction peaks of PANI, which we attributed to low PANI concentration and a lower XRD signal intensity compared with UiO-66-NH_2.

Nitrogen-sorption isotherm curves and the pore size distributions of UiO-66-NH_2, PANI, and UiO-66-NH_2@PANI are shown in Fig. S1 and S2 (ESI†). Brunauer–Emmett–Teller (BET) surface areas and pore volumes were derived from nitrogen adsorption isotherms at 77 K and the results are presented in Table 1. The BET surface area and total pore volume of UiO-66-NH_2 were calculated at 1384 $m^2\ g^{-1}$ and 1.18 $cm^3\ g^{-1}$, respectively, much higher than UiO-66-NH_2@PANI, which were 709 $m^2\ g^{-1}$ and 0.63 $cm^3\ g^{-1}$, respectively.

The presence of functional groups on PANI, UiO-66-NH_2, and UiO-66-NH_2@PANI can be identified by FTIR measurements. As shown in Fig. 2, the FTIR spectrum of PANI displayed

Table 1 BET surface areas and pore volumes of UiO-66-NH_2 and UiO-66-NH_2@PANI

Specimens	Surface area ($m^2\ g^{-1}$)	Pore volume ($cm^3\ g^{-1}$)
UiO-66-NH_2	1384	1.18
UiO-66-NH_2@PANI	709	0.63

absorption peaks at 1560, 1472, 1297, and 1117 cm^{-1}. The peaks at 1560 and 1472 cm^{-1} correspond to C=C stretching deformation of quinoid and benzene rings, revealing the presence of an emeraldine salt state in PANI.[30] The band at 1297 cm^{-1} was assigned to C–N stretching vibrations, and the bands at 1117 cm^{-1} was assigned to the quinonoid unit of doped PANI.[31,32] For the sample of UiO-66-NH_2, two obvious absorption peaks at 3477 and 3363 cm^{-1} were attributed to the asymmetric and symmetric vibrations of N–H bonding in the amino group. Moreover, the absorption bands at 1433 and 1655 cm^{-1} were related to the C=C from aromatic and the coordinated carboxylate moieties, respectively.[33] From the spectrum of UiO-66-NH_2@PANI, the absorption band at 1117 cm^{-1} is red shifted to 1135 cm^{-1} because of strong electrostatic interactions between PANI and UiO-66-NH_2.[31] Additionally, compared with pure PANI, the C=C stretching vibrations of the quinoid ring and benzenoid ring of the UiO-66-NH_2 is shifted from 1560 and 1472 cm^{-1} to 1570 and 1493 cm^{-1}, indicating an enhancement of π–π interactions between PANI and UiO-66-NH_2 frameworks.[30] Upon coating with PANI, the color of the UiO-66-NH_2 composites turned from yellow to green. The UV-vis spectra provided further evidence for this observation. PANI@UiO-66-NH_2 shows two absorptions at 273 and 377 nm respectively. Compared to the PANI curve, a considerable red shift from 350 to 377 nm is observed in the PANI@UiO-66-NH_2 composite due to the noncovalent π–π stacking between the phenyl rings of PANI and UiO-66-NH_2 (Fig. S3, ESI†). The Raman spectra show that the band at 1482 cm^{-1} was assigned to an in-plane deformation of the C–C bond of the quinoid ring of the doped PANI,

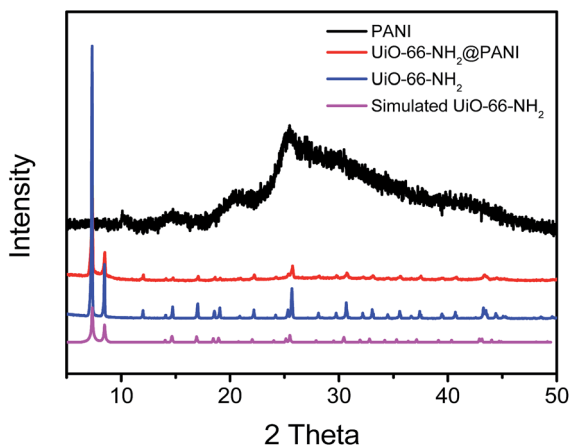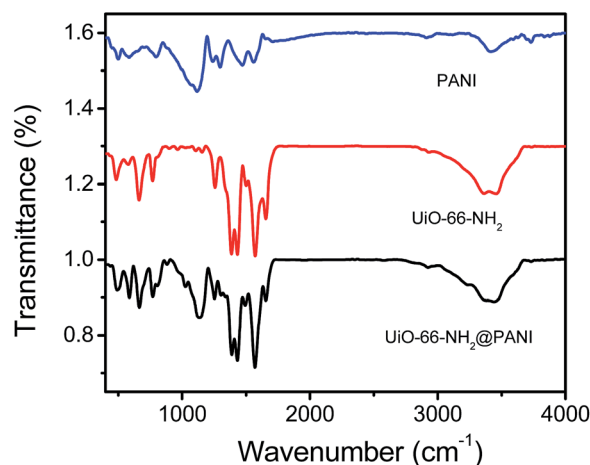**Fig. 1** Powder X-ray diffraction patterns of PANI, UiO-66-NH_2@PANI, UiO-66-NH_2, and simulated UiO-66-NH_2.

Fig. 2 FTIR transmission spectra of PANI, UiO-66-NH_2 and UiO-66-NH_2@PANI.
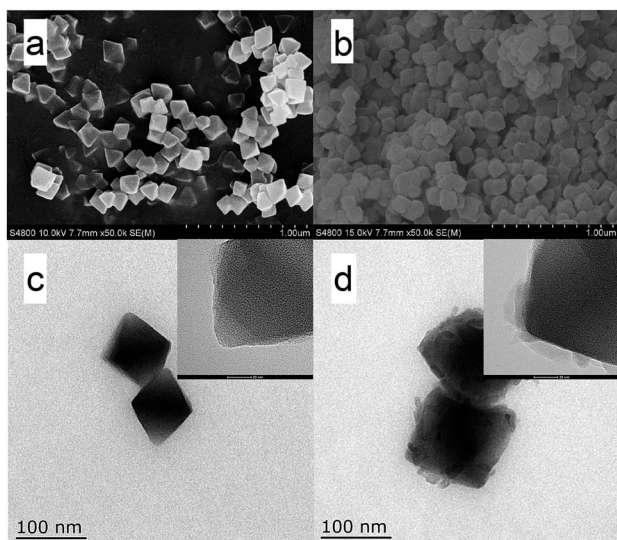
Fig. 3 SEM and TEM images of UiO-66-NH$_2$ (a and c) and UiO-66-NH$_2$@PANI (b and d).

which is shifted to 1490 cm^{-1} in the UiO-66-NH$_2$ due to π–π interactions between PANI and UiO-66-NH$_2$ (Fig. S4, ESI†). This is consistent with FTIR data.

Fig. 3 shows the SEM and TEM images of UiO-66-NH$_2$ and UiO-66-NH$_2$@PANI composites. It can be seen that, although the prepared UiO-66-NH$_2$ has more regular faceted surfaces than UiO-66-NH$_2$@PANI, both of them have a more discernible and better dispersion, which can facilitate the formation of a robust homogeneous film for the construction of an electrochemical sensor (Fig. 3a and b). The TEM image in Fig. 3c further confirms the formation of UiO-66-NH$_2$ with small octahedral cubic intergrown crystals. The TEM image in Fig. 3d clearly reveals the core@shell morphology of the UiO-66-NH$_2$@PANI composites with the outer layer of PANI and the inner core of UiO-66-NH$_2$, confirming the successful preparation of UiO-66-NH$_2$@PANI composites.

X-ray photoelectron spectroscopy (XPS) was employed to characterize the intrinsic oxidation state and protonation level of PANI formed in UiO-66-NH$_2$@PANI (Fig. 4). The N 1s spectrum of UiO-66-NH$_2$ can be decomposed into two distinct curves: one peak at 399.4 eV was assigned to –NH$_2$, and the other peak at 400.8 eV may be due to the interaction between the amidogen and proton (Fig. 4a).[34] The peaks at 398.3, 399.3, 400.5 and 401.9 eV in the spectrum of UiO-66-NH$_2$@-PANI correspond to the neutral and imine-like (=NH–) structure, neutral and amine-like nitrogen atoms (–NH–) and –NH$_2$, protonated imine (=NH$^+$–) and –NH$_3^+$, and protonated amine units (–NH$_2^+$–), respectively (Fig. 4b).[35–38] It is documented that the ratio of N$^+$/N could indicate the proton doping level of the polymer. According to quantitative analysis of the deconvoluted N (1s) spectra of UiO-66-NH$_2$@PANI, the ratio of –NH$_2^+$/N is 0.22. We could infer that the doping ratio of PANI in the UiO-66-NH$_2$@PANI should be far above 0.22, because UiO-66-NH$_2$ also contributes to benzenoid amine (–NH$_2$) and protonated imine (=NH$^+$–), which demonstrated that PANI could supply a path for electron conduction effectively.

Fig. 5 shows the TGA curves of UiO-66-NH$_2$ and UiO-66-NH$_2$@PANI. The first weight loss of UiO-66-NH$_2$ can be ascribed to the release of moisture and bound water from 50–150 °C. The second step of weight loss at 150–304 °C was due to dehydroxylation of OH$^-$ and was completed. The third step of weight loss was due to decomposition of material above 621 °C. From UiO-66-NH$_2$@PANI, it can be seen that the sharp weight loss begins near 121 °C, and continues till 621 °C, which is probably attributed to large-scale thermal degradation of polyaniline chains and UiO-66-NH$_2$. The last stage for both materials above 621 °C is related to the weight of Zr and residue. The weight percent of polyaniline is about 19.4% for UiO-66-NH$_2$@PANI. The energy dispersive spectroscopy (EDS) mapping images of Cl and Zr are shown in Fig. S5 (ESI†). The good dispersion of Cl element all over the support reveals the uniform distribution of PANI all over the support.
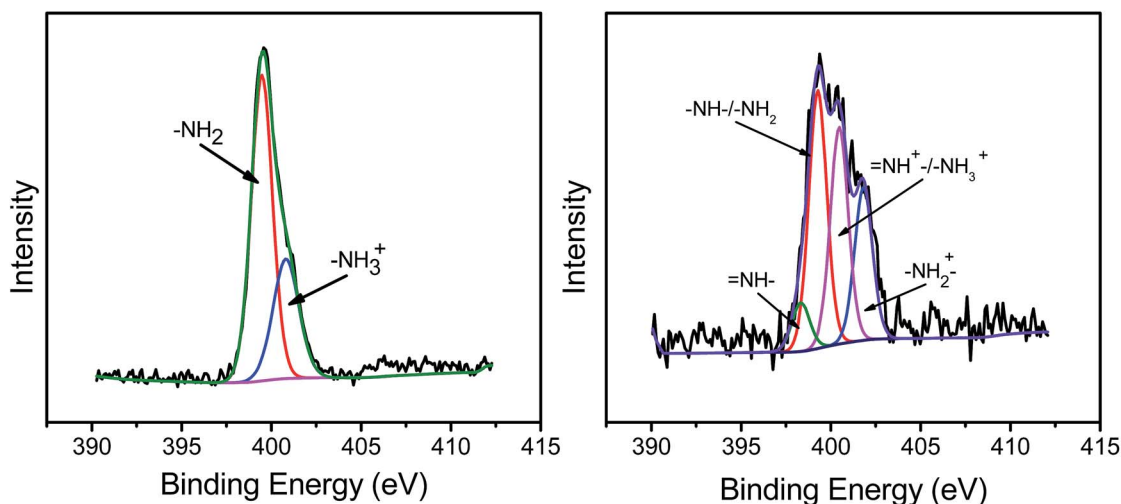

Fig. 4 N 1s XPS core-level spectra of the UiO-66-NH$_2$ (a) and UiO-66-NH$_2$@PANI (b).
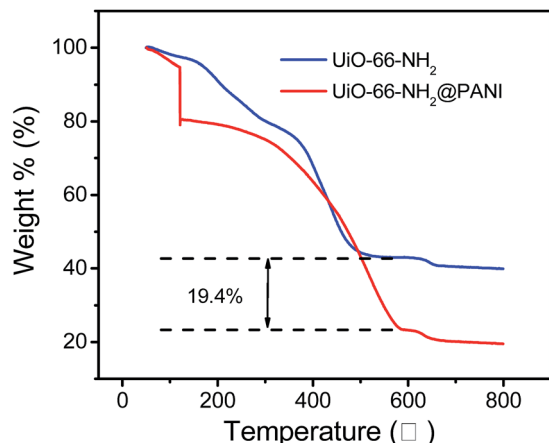
8388 | *J. Mater. Chem. A*, 2017, **5**, 8385–8393

This journal is © The Royal Society of Chemistry 2017

Fig. 5 TGA curves of UiO-66-NH$_2$ and UiO-66-NH$_2$@PANI.

3.2. Electrochemical behavior

Cyclic voltammetry (CV) and electrochemical impedance spectroscopy (EIS) were used to investigate the characteristics of different modified electrodes (bare GCE, UiO-66-NH$_2$/GCE and UiO-66-NH$_2$@PANI/GCE). CV was carried out in 1.0 mmol L^{-1} [Fe(CN)$_6$]$^{3-/4-}$ (1 : 1) solution containing 0.1 mol L^{-1} KCl. As shown in Fig. 6a, reversible redox peaks were obtained at the bare GCE. The relatively larger anodic and cathodic currents were observed, after the GCE was modified with UiO-66-NH$_2$, can be due to the large specific area and better conductivity. The CV response of the UiO-66-NH$_2$@PANI modified GCE showed the largest current signal, indicating that the cooperation of UiO-66-NH$_2$ and PANI accelerates the electron transfer and enhances the electrochemical sensitivity. EIS of [Fe(CN)$_6$]$^{3-/4-}$ is used to provide information about the interface properties and impedance changes in the process of electrode modification. Fig. 6b exhibits the Nyquist diagrams of the different modified electrodes. The bare GCE has a relative large electron-

transfer resistance (R_{ct}) value of about 246 Ω. At the UiO-66-NH$_2$/GCE, the value of resistance was changed to 160 Ω, suggesting that the bare GCE was coated efficiently by UiO-66-NH$_2$. A distinct decrease in the interfacial electron transfer resistance was also observed when PANI was coated on the out surface of MOFs (76 Ω), indicating that PANI with superior electrical conductivity can accelerate the electron transfer on the electrode.

In order to study the mass transfer process of the modified electrode, CVs of the UiO-66-NH$_2$@PANI modified electrode at various scan rates are shown in Fig. 7. Both anodic and cathodic current responses increased linearly with the square root of scan rate ($v^{1/2}$) in the range of 20–130 mV s^{-1}, it can be expressed as the Randle–Sevick equation:[39]
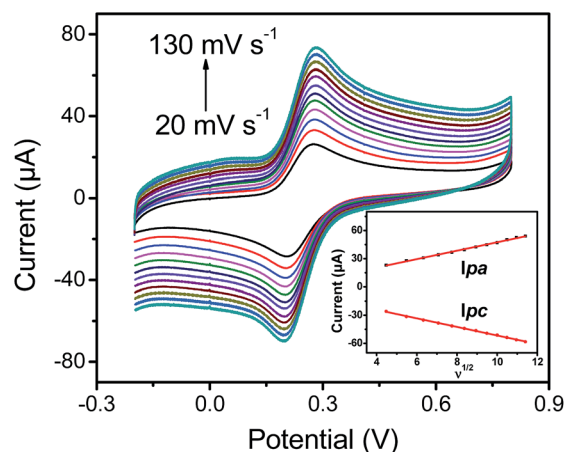

Fig. 7 Cyclic voltammograms of the UiO-66-NH$_2$@PANI electrode in 0.1 mol L^{-1} KCl solution containing 1 mmol L^{-1} Fe(CN)$_6$$^{3-/4-}$ at different scan rates of 20, 30, 40, 50, 60, 70, 80, 90, 100, 110, 120, and 130 mV s^{-1}. Inset: dependence of the redox peak current on the scan rate.
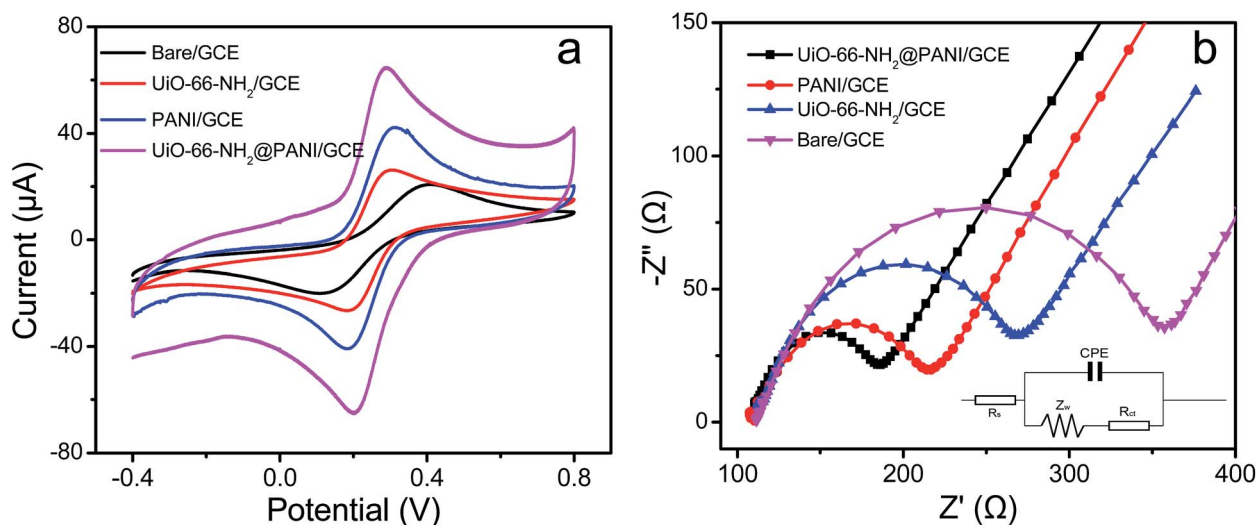

Fig. 6 Cyclic voltammetry diagrams (a) and electrochemical impedance spectra (b) of the glassy carbon electrode, UiO-66-NH$_2$/GCE and UiO-66-NH$_2$@PANI/GCE in a 0.1 mol L^{-1} KCl solution containing 1.0 mmol L^{-1} [Fe(CN)$_6$]$^{3-/4-}$.

This journal is © The Royal Society of Chemistry 2017

J. Mater. Chem. A, 2017, **5**, 8385–8393 | 8389

$$I = (2.69 \times 10^5)n^{3/2}ACD^{1/2}v^{1/2}$$

where the constant n is the number of transferred electrons, A is the electrode surface area (cm^2), C is the concentration of the electroactive species (mol cm^{-3}), D is the diffusion coefficient of $[Fe(CN)_6]^{3-/4-}$ equal to 6.70×10^{-7} cm^2 s^{-1}, and v is the scan rate (V s^{-1}).

As shown in Fig. 7 (inset), the linearity of peak currents *versus* the square root of the scan rate with correlation coefficients (R^2) of 0.9978 and 0.9989 was achieved for both anodic and cathodic peak currents, indicating that diffusion controlled mass transfer process occurs on the UiO-66-NH$_2$@PANI modified GCE.

The electrochemical responses of 100 μg L^{-1} Cd(II) in 0.1 mol L^{-1} ABS (pH = 5.0) at different electrodes were investigated using DPV. As shown in Fig. 8, a small oxidation peak was observed at the bare GCE. When UiO-66-NH$_2$ was coated on the electrode surface, the oxidation peak current increased significantly. Improved results were also obtained using the UiO-66-NH$_2$@PANI/GCE. The oxidation peak current was larger than those of the two electrodes before. This is because PANI can increase the conduction pathways and promote the electron transfer between the solution and electrode surface. In addition, the UiO-66-NH$_2$@PANI modified GCE showed well-defined peaks and an almost 10-fold current increase response to Cd(II), which is credited to the synergistic amplification effect of UiO-66-NH$_2$ with PANI.

The solution pH is one of the most important parameters influencing the adsorption process of metal ions on the electrode materials because of the protonation or deprotonation reaction for the electrode materials or the hydrolysis reaction for the metal ions under alkaline conditions. In this experiment, the solution pH was varied over the range of 3.0 to 7.0. As shown in Fig. S6 (ESI†), the current intensity increased with the increase of the solution pH and declined gradually with further increase in pH up to 7.0. These observations allow us to propose
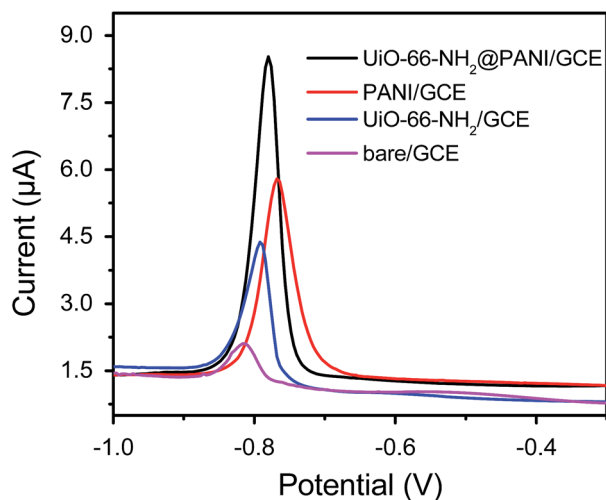
that at low pH, the protonated amino groups (–NH$_3^+$) repulse cations *via* electrostatic repulsion, and with increasing pH, the protonated amino groups decreased; thus electrostatic attraction resulted in a higher stripping current of cadmium. The best signal intensity was reached at pH 5.0. As shown in Fig. S7 (ESI†), the zeta potential value of UiO-66-NH$_2$@PANI decreases with the increase of solution pH, and the isoelectrical point is calculated to be 4.4. In addition, the hydrolysis degree of the metal ions increases along with the increasing of pH, and white Cd(OH)$_2$ precipitate was formed. Then pH 5.0 was chosen for further studies.

In electrochemical determination, accumulation is an effective and simple way to improve the determining sensitivity. In this work, the effects of accumulation potential and time on the oxidation peak current of Cd(II) were investigated. It was found that the oxidation peak current of Cd(II) initially increased, obviously by changing accumulation potential from −1.6 to −1.2 V and then gradually decreased from −1.2 to −0.6 V (Fig. S8, ESI†). Thus the accumulation potential of −1.2 V was chosen as the optimum accumulation potential for further experiments. Moreover, the oxidation peak current is very low without accumulation (0 s). With gradually increasing the accumulation time from 0.0 to 120 s (Fig. S9, ESI†), the oxidation peak current almost linearly increases. With increasing the accumulation time, more and more cadmium accumulates at the UiO-66-NH$_2$@PANI/GCE surface, so the oxidation peak current greatly increases. However, the oxidation peak current almost remains constant when the accumulation time is longer than 120 s, suggesting that the amount of cadmium at the UiO-66-NH$_2$@PANI electrode surface tends to saturate. Considering both sensitivity and working efficiency, an accumulation time of 120 s was selected.

3.3.   Differential pulse voltammetric determinations

Fig. 9 shows the DPV curves of Cd(II) at the UiO-66-NH$_2$@PANI/GCE at various concentrations. The oxidation peak currents are proportional to the concentration of Cd(II) in a wider range of 0.5 to 600 μg L^{-1}. The linear equation is I (μA) = 0.06117 C (μg L^{-1}) + 0.49938 (R^2 = 0.9968), and the detection limit is as low as 0.3 μg L^{-1} (S/N = 3). As shown in Table 2, compared with those obtained by other reported electrochemical methods, the proposed method has the lowest detection limit as well as a wider linear range.[40–55] The repeatability of the modified electrode was investigated by the analysis of 10 μg L^{-1} Cd(II) for 6 repetitive measurements, and the relative standard deviation (R.S.D.) for the oxidation peak currents was 3.9%, indicating excellent repeatability of the modified electrode. The fabrication reproducibility was estimated with five different electrodes constructed independently by the same procedure. The R.S.D. of 4.5% was obtained, which demonstrated the reliability of the fabrication procedure. The long-term stability of the UiO-66-NH$_2$@PANI/GCE was further investigated. It was found that the prepared UiO-66-NH$_2$@PANI composites were relatively stable up to at least 10 cycles with 95.1% of the initial current response. The excellent sensor performance is due to the structural properties of UiO-66-NH$_2$: (1) the large surface area of
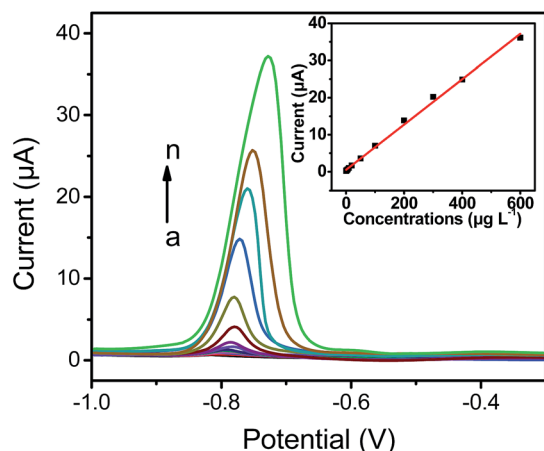

Fig. 8   Differential pulse voltammograms of 100 μg L^{-1} Cd(II) at the bare GCE and GCEs modified with UiO-66-NH$_2$, PANI and UiO-66-NH$_2$@PANI in 0.1 mol L^{-1} ABS (pH = 5.0).

Fig. 9 Differential pulse voltammograms of cadmium at the UiO-66-NH_2@PANI modified electrode in the pH 5.0 ABS. Cadmium concentrations (from a to n): 0.5, 0.8, 1, 3, 5, 6, 10, 20, 50, 100, 200, 300, 400 and 600 μg L^{-1}. The inset shows the relationship between peak current and cadmium concentration.

Table 2 Comparison of the analytical performance with other methods using different electrode materials for the determination of Cd(II)[a]

Modified electrode	Detection limit (μg L^{-1})	Linear range (μg L^{-1})	Ref.
G/PANI/PS nanoporous fiber/SPCE	4.4	10–500	40
SPAN/MCN/GCE	0.7	5–80	41
Diacetyldioxim/CPE	4.5	28.1–2810	42
RGO/Bi/GCE	2.8	20–120	43
Bi/CNT/SPCE	0.7	2–100	44
Polymeric Nafion/Bi/GCE	2.0	2–60	45
TiO_2/ZrO_2 composite/CPE	0.8	1–200	46
Bi/CNT/SPCE	0.8	2–100	47
ERGNO/Bi film/SPCE	0.5	1–60	48
(C–Bi) nanocomposite/CPE	0.6	1–100	49
Bi/poly(p-ABSA)/GCE	0.6	1–110	50
Nafion/Bi/NMC/GCE	1.5	2–10, 10–100	51
PA/PPy/GO/GCE	2.1	5–150	52
Penicillamine/GCE	4.3	14.3–115.2	53
Bi/Nafion/GCE	0.4	5.0–60.0	54
SNAC/GCE	2.7	18.6–1181.0	55
UiO-66-NH_2@PANI/GCE	0.3	0.5–600	This work

[a] SPAN: self-doped polyaniline; MCN: mesoporous carbon nitride; G: graphene; PS: polystyrene; SPCE: screen-printed carbon electrode; CPE: carbon paste electrode; GO: graphene oxide; RGO: reduced graphene oxide; Bi: bismuth; ERGNO: electrochemically reduced graphene oxide; Cys: cysteine; poly(p-ABSA): poly(p-aminobenzene sulfonic acid); NMC: nitrogen-doped microporous carbon; PA: phytic acid; PPy: polypyrrole; SNAC: spherical carbon nanoparticle decorated activated carbon.

UiO-66-NH_2 can offer more adsorption sites and improves the electrochemical response. (2) UiO-66-NH_2 exhibited high resistance toward many chemicals, and it retains full crystallinity even after being coated with PANI in hydrochloric acid. (3) The incorporation of amine functionality into the UiO-66 structure

Table 3 Determination of Cd(II) in real samples and its spiked recovery

Sample	Spiked (μg L^{-1})	Found (μg L^{-1})	Recovery%
Lake water	0.00	3.60	—
	2.00	5.54	97.0
	5.00	8.69	101.8
Tap water	0.00	1.91	—
	2.00	3.96	102.5
	5.00	6.98	101.4
Saliva	0.00	—	—
	2.00	2.06	103.0
	5.00	4.97	99.4
Urine	0.00	1.01	—
	2.00	2.96	97.5
	5.00	6.14	102.6

hadn't lost the chemical stability of MOF, and the sensor can be reused many times in aqueous solution.

3.4. Influence of co-existing ions and analysis application

In order to demonstrate the selectivity of the sensor, the interference study was carried out by the standard addition of commonly existing cations and anions into the electrochemical cell containing 10 μg L^{-1} of Cd(II). The tolerance level as the relative error did not exceed ± 5%, and the results are summarized in Table S1 (ESI†). We can see that the proposed sensor showed no obvious interference from most of the common ions due to the specific and selective interaction between the modifier functionalities and the Cd(II) ions. However, Cd(II) stripping peak current decreased when the concentrations of Cu(II) were more than 50 μg L^{-1}, probably due to the competition between Cu(II) and Cd(II) at the active sites. Similar results were reported in the literature.[40,41,44,50–54] Moreover, Hg(II) was found to enhance the current intensity of Cd(II) due to the formation of an amalgam on the electrode with Cd(II) at the concentration of 50 μg L^{-1}.

The feasibility of the proposed sensor was validated by analyzing Cd(II) in lake water, tap water, saliva and urine samples. The analytical results along with the recoveries by spiking Cd(II) with the samples are given in Table 3. As can be seen, recoveries of 97.0–103.0% were achieved for all the spiked samples. The results suggested that the UiO-66-NH_2@PANI modified GCE was very reliable and sensitive enough for the determination of Cd(II) in real environmental and biological samples.

4. Conclusions

We showed that a UiO-66-NH_2@PANI composite with a core/shell structure was synthesized successfully *via* a simple hydrothermal approach followed by PANI coatings. Under optimized experimental conditions, the prepared UiO-66-NH_2@PANI composite modified electrode was applied for the detection of trace levels of cadmium ions by differential pulse stripping voltammetry. Compared with existing cadmium ions sensors, the UiO-66-NH_2@PANI modified electrode

showed the lowest detection limit at 0.3 µg L^{-1}, a wider linear range, and better stability and repeatability. This can be attributed to the fact that both the core and shell materials are good electrode materials and their novel properties containing the characteristics of each of the components could promote the quality of the sensor. The practical application was demonstrated by determination of cadmium ions in real samples. All of these features suggest that our conductive polymer coated MOFs will lead to an exciting future and intriguing discoveries of MOF-based electrochemical sensors for environmental monitoring and clinical diagnostics. Besides, high selective functional groups (such as sulfhydryl group for mercury) should be developed to improve the selectivity of the method for the analysis target analytes in a complicated matrix.

Acknowledgements

References

1 P. Pohl, *Trends Anal. Chem.*, 2009, **28**, 117–128.

2 G. Zhou, X. Xu, W. Zhu, B. Feng and J. Hu, *New J. Chem.*, 2015, **39**, 7355–7362.

3 S. Wen, X. Zhu, Q. Huang, H. Wang, W. Xu and N. Zhou, *Microchim. Acta*, 2014, **181**, 1041–1047.

4 M. Merin, M. Anke and M. S. Ihnat, *Elements and their compounds in the environment: occurrence, analysis and biological relevance*, Wiley VCH Verlag GmbH & KGaA, Weinhein, 2004.

5 D. Saha, S. Barakat, B. S. E. Van, K. A. Nelson, D. K. Hensley and J. Chen, *ACS Appl. Mater. Interfaces*, 2016, **8**(49), 34132–34142.

6 J. M. Mo, L. Zhou, X. H. Li, Q. Li, L. J. Wang and Z. Wang, *Microchem. J.*, 2017, **130**, 353–359.

7 H. W. Choi, K. H. Lee, N. H. Hur and H. B. Lim, *Anal. Chim. Acta*, 2014, **847**, 10–15.

8 K. M. Zeinu, H. Hou, B. Liu, X. Yuan, L. Huang, X. Zhu, J. Hu, J. Yang, S. Liang and X. Wu, *J. Mater. Chem. A*, 2016, **4**, 13967–13979.

9 F. C. Anson and D. J. Barclay, *Anal. Chem.*, 1968, **40**, 1791–1798.

10 H. B. Herman, R. L. McNeely, P. Surana, C. M. Elliott and R. W. Murray, *Anal. Chem.*, 1974, **46**, 1258–1265.

11 Z. Yang, X. Huang, R. Zhang, J. Li, Q. Xu and X. Hu, *Electrochim. Acta*, 2012, **70**, 325–330.

12 O. K. Farha and J. T. Hupp, *Acc. Chem. Res.*, 2010, **43**, 1166–1175.

13 D. Zhao, D. J. Timmons, D. Q. Yuan and H. C. Zhou, *Acc. Chem. Res.*, 2010, **44**, 123–133.

14 B. Seoane, J. Coronas, I. Gascon, M. Etxeberria Benavides, O. Karvan, J. Caro, F. Kapteijn and J. Gascon, *Chem. Soc. Rev.*, 2015, **44**, 2421–2454.

15 J. L. C. Rowsell and O. M. Yaghi, *J. Am. Chem. Soc.*, 2006, **128**, 1304–1315.

16 K. Schlichte, T. Kratzke and S. Kaskel, *Microporous Mesoporous Mater.*, 2004, **73**, 81–88.

17 B. Liu and B. Smit, *J. Am. Chem. Soc.*, 2009, **25**, 5918–5926.

18 Y. Wang, H. Ge, G. Ye, H. Chen and X. Hu, *J. Mater. Chem. B*, 2015, **3**, 3747–3753.

19 Y. Zhang, X. Bo, C. Luhana, H. Wang, M. Li and L. Guo, *Chem. Commun.*, 2013, **49**, 6885–6887.

20 Y. Wang, L. Wang, H. Chen, X. Hu and S. Ma, *ACS Appl. Mater. Interfaces*, 2016, **8**, 18173–18181.

21 Z. Xu, L. Yang and C. Xu, *Anal. Chem.*, 2015, **87**, 3438–3444.

22 F. Y. Kong, S. X. Gu, W. W. Li, T. T. Chen, Q. Xu and W. Wang, *Biosens. Bioelectron.*, 2014, **56**, 77–82.

23 S. Miura, H. Naito, Y. Kanemitsu, Y. Matsuura, K. Matsukawa and H. Inoue, *Thin Solid Films*, 2003, **438–439**, 253–256.

24 K. Hosono, I. Matsubara, N. Murayama, S. Woosuck and N. Izu, *Chem. Mater.*, 2005, **17**, 349–354.

25 J. Gong, Y. Li, Z. Hu, Z. Zhou and Y. Deng, *J. Phys. Chem. C*, 2010, **114**, 9970–9974.

26 B. A. Bhanvase, N. S. Darda, N. C. Veerkar, A. S. Shende, S. R. Satpute and S. H. Sonawane, *Ultrason. Sonochem.*, 2015, **24**, 87–97.

27 M. Kandiah, M. H. Nilsen, S. Usseglio, S. Jakobsen, U. Olsbye, M. Tilset, C. Larabi, E. A. Quadrelli, F. Bonino and K. P. Lillerud, *Chem. Mater.*, 2010, **22**, 6632–6640.

28 L. Shen, S. Liang, W. Wu, R. Liang and L. Wu, *J. Mater. Chem. A*, 2013, **1**, 11473–11482.

29 M. U. A. Prathap, R. Srivastava and B. Satpati, *Electrochim. Acta*, 2013, **114**, 285–295.

30 S. Wang, L. Ma, M. Gan, S. Fu, W. Dai, T. Zhou, X. Sun, H. Wang and H. Wang, *J. Power Sources*, 2015, **299**, 347–355.

31 S. Dhibar and C. K. Das, *J. Alloys Compd.*, 2015, **653**, 486–497.

32 T. Yang, R. Yang, H. Chen, F. Nan, T. Ge and K. Jiao, *ACS Appl. Mater. Interfaces*, 2015, **7**, 2867–2872.

33 M. Vahidi, A. Tavasoli and A. M. Rashidi, *J. Nat. Gas Sci. Eng.*, 2016, **28**, 651–659.

34 Q. Chen, Q. He, M. Lv, Y. Xu, H. Yang, X. Liu and F. Wei, *Appl. Surf. Sci.*, 2015, **327**, 77–85.

35 S. B. Aliev, D. G. Samsonenko, E. A. Maksimovskiy, E. O. Fedorovskaya, S. A. Sapchenko and V. P. Fedin, *New J. Chem.*, 2016, **40**, 5306–5312.

36 C. C. Hu and J. Y. Lin, *Electrochim. Acta*, 2002, **47**, 4055–4067.

37 W. A. Marmisollé and O. Azzaroni, *Nanoscale*, 2016, **8**, 9890–9918.

38 L. Wang, X. Feng, L. Ren, Q. Piao, J. Zhong, Y. Wang, H. Li, Y. Chen and B. Wang, *J. Am. Chem. Soc.*, 2015, **137**, 4920–4923.

39 A. J. Bard and L. R. Faulkner, *Electroanalytical methods*, Wiley, New York, 1980.

40 N. Promphet, P. Rattanarat, R. Rangkupan, O. Chailapakul and N. Rodthongkum, *Sens. Actuators, B*, 2015, **207**, 526–534.

41 C. Zhang, Y. Zhou, L. Tang, G. Zeng, J. Zhang, B. Peng, X. Xie, C. Lai, B. Long and J. Zhu, *Nanomaterials*, 2016, **6**, 7–11.

42 C. Hu, K. Wu, X. Dai and S. Hu, *Talanta*, 2003, **60**, 17–24.

43 P. K. Sahoo, B. Panigrahy, S. Sahoo, A. K. Satpati, D. Li and D. Bahadur, *Biosens. Bioelectron.*, 2013, **43**, 293–296.

44 G. H. Hwang, W. K. Han, J. S. Park and S. G. Kang, *Talanta*, 2008, **76**, 301–308.

45 G. Kefala and A. Economou, *Anal. Chim. Acta*, 2006, **576**, 283–289.

46 P. K. Q. Nguyen and S. K. Lunsford, *J. Electroanal. Chem.*, 2013, **711**, 45–52.

47 U. Injang, P. Noyrod, W. Siangproh, W. Dungchai, S. Motomizu and O. Chailapakul, *Anal. Chim. Acta*, 2010, **668**, 54–60.

48 J. Ping, Y. Wang, J. Wu and Y. Ying, *Food Chem.*, 2014, **151**, 65–71.

49 M. Gich, C. F. Sánchez, L. C. Cotet, P. Niu and A. Roig, *J. Mater. Chem. A*, 2013, **1**, 11410–11418.

50 Y. Wu, N. B. Li and H. Q. Luo, *Sens. Actuators, B*, 2008, **133**, 677–681.

51 L. Xiao, H. Xu, S. Zhou, T. Song, H. Wang, S. Li, W. Gan and Q. Yuan, *Electrochim. Acta*, 2014, **143**, 143–151.

52 H. Dai, N. Wang, D. Wang, H. Ma and M. Lin, *Chem. Eng. J.*, 2016, **299**, 150–155.

53 C. P. Rafols, N. Serrano, J. M. D. Cruz, C. Arino and M. Esteban, *Talanta*, 2015, **144**, 569–573.

54 D. Yang, L. Wang, Z. Chen, M. Megharaj and R. Naidu, *Microchim. Acta*, 2014, **181**, 1199–1206.

55 R. Madhu, K. V. Sankar, S. M. Chen and R. K. Selvan, *RSC Adv.*, 2014, **4**, 1225–1233.